New Journal of Physics
The open access journal at the forefront of physics

PAPER • OPEN ACCESS

Edge state mimicking topological behavior in a one-dimensional electrical circuit

To cite this article: Shuo Liu *et al* 2021 *New J. Phys.* **23** 103005

New Journal of Physics
The open access journal at the forefront of physics

Deutsche Physikalische Gesellschaft DPG
IOP Institute of Physics

Published in partnership with: Deutsche Physikalische Gesellschaft and the Institute of Physics

OPEN ACCESS

RECEIVED
30 March 2021

REVISED
26 August 2021

ACCEPTED FOR PUBLICATION
16 September 2021

PUBLISHED
6 October 2021

PAPER

Edge state mimicking topological behavior in a one-dimensional electrical circuit

Shuo Liu[1], Shaojie Ma[2,*], Ruiwen Shao[3], Lei Zhang[3], Biao Yang[4], Miguel Navarro-Cía[1,5,*], Tie Jun Cui[3,*] and Shuang Zhang[2,*]

[1] School of Physics and Astronomy, University of Birmingham, Birmingham B15 2TT, United Kingdom
[2] Physics Department, The University of Hong Kong, Pokfulam Road, Hong Kong, People's Republic of China
[3] State Key Laboratory of Millimeter Waves, Southeast University, Nanjing 210096, People's Republic of China
[4] Department of Physics and Institute for Advanced Study, The Hong Kong University of Science and Technology, Hong Kong, People's Republic of China
[5] Department of Electronic, Electrical and Systems Engineering, University of Birmingham, Birmingham B15 2TT, United Kingdom
[*] Authors to whom any correspondence should be addressed.

E-mail: shaojiema90@gmail.com, M.Navarro-Cia@bham.ac.uk, Tjcui@seu.edu.cn and S.Zhang@bham.ac.uk

Keywords: topological insulator, electrical circuit, edge stage

Supplementary material for this article is available online

Abstract

For one-dimensional (1D) topological insulators, the edge states always reside in the bulk bandgaps as isolated modes. The emergence and vanishing of these topological edge states are always associated with the closing/reopening of the bulk bandgap and changes in topological invariants. In this work, we discover a special kind of edge state in a 1D electrical circuit, which can appear not only inside the bandgap but also outside the bulk bands with the changing of bulk circuit parameters, resembling Tamm states or Shockley states. We prove analytically that the emergence/vanishing of this edge state and its position relative to the bulk bands depends on the intersections of certain critical frequencies. Specifically, the edge mode in the proposed circuit can be mathematically described by polynomials with roots equal to some critical frequencies in the bulk circuit. From this point of view, the transition of the edge state is uniquely determined by the order of the critical frequencies in the bulk circuit. Such topological behaviors shown by the edge state in the proposed electrical circuit may indicate, in a broader sense, the presence of certain type of topology.

1. Introduction

Edge states, or surface states, appearing at a material interface, have been observed in in various physical systems. They can be classified into trivial and nontrivial phases, depending on whether they possess certain nontrivial topologies in the bulk. For topological edge states, they always appear either as isolated modes inside the bandgap of one-dimensional (1D) topological systems, or as continuous lines/surfaces between the bulk bands in two-dimensional (2D)/three-dimensional (3D) topological systems. The emergence and vanishing of them are always accompanied by the closing and reopening of bulk bandgap and are related to changes in the topological invariant of the bulk system. This is known as the bulk-edge correspondence [1–3], which ensures a one-to-one correspondence between the number of topological edge states in an open system and the topological invariant in the bulk. Meanwhile, trivial edge states, commonly known as the Tamm states [4] or Shockley states [5], do not present such topological behavior. Their existence is highly related to the boundary properties and can appear almost everywhere in the band structure, even inside the bulk band as the bound states in the continuum [6, 7].

Electrical circuits [8] have recently emerged as a popular platform for studying various topological states, covering a wide range of designs from 1D [9, 10], 2D [11–16], 3D [17, 18], to 4D [19–21], from Hermitian [9, 11–14, 17, 19, 21] to non-Hermitian [14, 18, 22, 23], from topological insulators

[11, 13, 14, 17] to topological semimetals [24–26], from lower-order to higher-order [14, 27, 28], and from linear to nonlinear regimes [29–31]. Electrical circuits are unique compared to the photonic and quantum electronic systems for the experimental investigation of topological physics in the following aspects. Firstly, low frequency electrical circuits provide high-precision experimental implementation to deliver highly accurate measurement results, due to the low parasitic effects of circuit wiring and high precision circuit component. Secondly, electrical circuits offer high degrees of freedom to the realization of exotic topological structures with complex couplings such as higher-dimensional and non-abelian type topological insulators [32–35], owing to the convenient connections among circuit nodes at an arbitrary distance. Thirdly, a wide range of active and nonlinear circuit components allows the experimental realization of non-Hermitian [15, 22, 23] and nonlinear topological systems [29–31] which possess much richer physics than the Hermitian counterpart.

In this work, we discover a special type of edge state in a 1D electrical circuit which displays certain topological behaviors. Distinct from conventional topological systems, we found that the edge state can traverse the bulk bands by varying only the bulk circuit parameters, i.e. they can appear not only inside the bulk bandgap, but also below or above the bulk bands. Most importantly, the emergence/vanishing of the edge states as well as their transition among the bulk bands is strictly determined by the competition of certain critical frequencies of the bulk circuit. That is to say, the transition of the surface state can only occur at the crossings of these critical bulk frequencies, making the circuit an analog of a topological insulator. The transport of edge state through the bulk bands is experimentally demonstrated through the measurement of the bulk and edge states in the circuit along a sweeping path in three different phase diagrams.

We note that the edge state observed in the proposed circuit belongs to the category of Tamm state. Although there have been literatures reported on the manipulation of the position of the Tamm states, or Shockley states, to be above or below the bulk bands [36–38], the boundary sites or the defect sites where the surface states appear have been intentionally modified. It is important to note that, in the circuit we proposed, the boundary sites are kept the same as the bulk sites, which forms a natural boundary truncation.

2. Circuit design and phase analysis

Each unit cell of the circuit comprises two resonators and two identical coupling links, as shown in figure 1(a). The grounded resonators are composed of a shunt-resonant circuit with inductors L_a/L_b and capacitors C_a/C_b, and the coupling links are made of identical shunt-resonant circuits with L_0 and C_0. We remark that this circuit is different from the Su–Schrieffer–Heeger (SSH) type topological circuit reported previously [11, 29, 30], in that both the on-site and coupling terms in our circuit are made of parallel resonant LC tanks, while in previous designs, the coupling terms are made of a single inductor or capacitor.

For the above circuit unit cell in the periodic boundary condition, we have the following Kirchhoff's current law circuit equations at the two nodes,

$$I_1 - \mathrm{i}\omega C_0 \cdot \left(V_2\,\mathrm{e}^{-\mathrm{i}k} - V_1\right) = I_a - \mathrm{i}\omega C_a \cdot V_1 + I_2 - \mathrm{i}\omega C_0 \cdot (V_1 - V_2) \tag{1}$$

$$I_2 - \mathrm{i}\omega C_0 \cdot (V_1 - V_2) = I_b - \mathrm{i}\omega C_b \cdot V_2 + I_1\,\mathrm{e}^{\mathrm{i}k} - \mathrm{i}\omega C_0 \cdot \left(V_2 - V_1\,\mathrm{e}^{\mathrm{i}k}\right) \tag{2}$$

and the Kirchhoff's voltage law circuit equations in the four loops as,

$$\begin{aligned} -\mathrm{i}\omega L_0 \cdot I_1 &= V_2\,\mathrm{e}^{-\mathrm{i}k} - V_1 & -\mathrm{i}\omega L_0 \cdot I_2 &= V_1 - V_2 \\ -\mathrm{i}\omega L_a \cdot I_a &= V_1 & -\mathrm{i}\omega L_b \cdot I_b &= V_2 \end{aligned} \tag{3}$$

in which V_1/V_2 are the voltage at node 1/2, I_1/I_2 are the current flowing through the coupling branches O_1/O_2, I_a/I_b are the current flowing through the resonator branches A/B, ω is the angular frequency, k is the quasi-wavevector. By defining $E = \omega^2 C_0 L_0$, $C_i = r_i C_0$, $L_i = s_i L_0$, $t_i = r_i s_i$, we can rewrite equations (1)–(3) in a dimensionless form as (see supplementary materials note S1 (https://stacks.iop.org/NJP/23/103005/mmedia)),

$$\boldsymbol{S}(k) \cdot \boldsymbol{V} = \boldsymbol{E} \cdot \boldsymbol{R}(k) \cdot \boldsymbol{V} \tag{4}$$

in which,

$$\boldsymbol{S}(k) = \begin{bmatrix} 2 + s_a^{-1} & -1 - \mathrm{e}^{-\mathrm{i}k} \\ -1 - \mathrm{e}^{\mathrm{i}k} & 2 + s_b^{-1} \end{bmatrix}, \qquad \boldsymbol{R}(k) = \begin{bmatrix} 2 + r_a & -1 - \mathrm{e}^{-\mathrm{i}k} \\ -1 - \mathrm{e}^{\mathrm{i}k} & 2 + r_b \end{bmatrix}, \qquad \boldsymbol{V} = \begin{bmatrix} V_1 \\ V_2 \end{bmatrix} \tag{5}$$

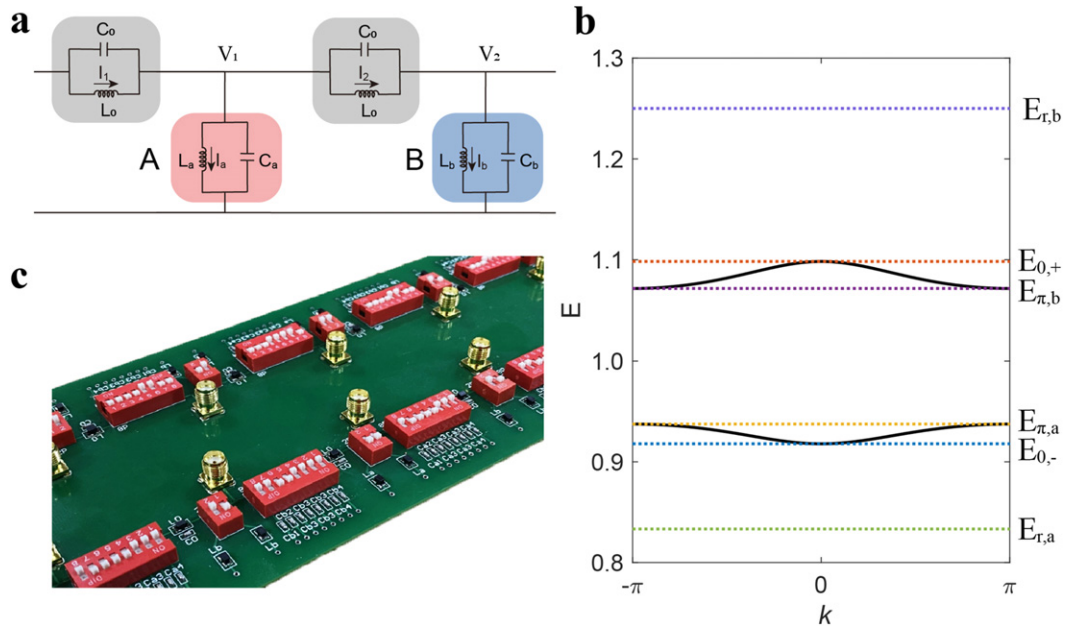

Figure 1. Structure and bulk band structure of the proposed circuit. (a) Circuit schematic of a single unit cell. (b) Fabricated sample with 10.5 (21 circuit node) unit cells. (c) Band structure of the bulk circuit with $r_a = 1.2$, $r_b = 1.8$, $s_a = s_b = 1$. The dashed lines mark the six critical frequencies of the bulk circuit.

Noted that by choosing a proper gauge $\boldsymbol{V} = \boldsymbol{R}^{1/2}\boldsymbol{V}$, we can have a Hermitian circuit Hamiltonian $\boldsymbol{H}(k) = \boldsymbol{R}^{-1/2}(k)\,\boldsymbol{S}(k)\,\boldsymbol{R}^{-1/2}(k)$.

Figure 1(b) shows the bulk band structure of a typical circuit with parameter $s_a = 1$, $s_b = 1$, $r_a = 1.2$, $r_b = 0.8$. The six dashed lines in the plot mark two resonant frequencies of the A/B branches $E_{r,a} = 1/t_a$, $E_{r,b} = 1/t_b$, and four frequency limits of the bulk bands, $E_{\pi,a} = \frac{1+2s_a}{2s_a+t_a}$, $E_{\pi,b} = \frac{1+2s_b}{2s_b+t_b}$, $E_{0,\pm} = \frac{s_a r_a + s_b r_b + 2s_a + 2s_b + 2s_a s_b (r_a + r_b) \pm \sqrt{\Delta_1}}{2s_a s_b \cdot (2r_a + 2r_b + r_a r_b)}$, in which Δ_1 is a positive real number (see supplementary materials note S1). The upper/lower bounds of the bulk bands $E_{\pi,a}$, $E_{\pi,b}$ depends only on the resonant frequencies of the A/B links, while the bounds of the bandgap $E_{0,+}$, $E_{0,-}$ depend on all circuit parameters. Crossing among the six critical frequencies can occur as the parameters s_a, s_b, r_a, r_b are tuned. We will see in the following demonstrations that the relative relations between these critical frequencies can determine the edge states of the system, that is, the number of edge modes and its position in the open circuit.

To investigate the edge state in such an electrical circuit, we consider a finite circuit chain with 50.5 unit cells (i.e. 101 circuit nodes), in which both boundaries are terminated with resonator B. We first consider the simple case with $s_a = s_b = 1$. Figure 2(a) shows the phase diagram of the circuit for $[r_a, r_b]$ ranging from 0 to 2. Two critical lines $r_b = r_a$, $r_b = 1$, divide the phase diagram into three regions, each representing an individual state describing a distinct location of the edge state relative to the bulk bands. The square bracket representation [1/0, 1/0, 1/0] indicates the existence/absence of edge state below, inside, and above the bulk band. For example, the yellow region marked with [0,1,0] represents an in-gap edge state which is located between the lower and upper bands; while the [1,0,0] and [1,0,0] regions represent a bottom and top edge state which reside below or above the bulk bands. To observe how the edge state crosses through the two bulk bands, we provide in figures 2(b)–(e) the variation of the band structure along four straight lines in the phase diagram (figure 2(a)), respectively, at $r_a = 0.5$, $r_a = 1.5$, $r_b = 0.5$, and $r_b = 1.5$, as marked by gray-dashed lines. The black dots in figures 2(b)–(e) represent the bulk modes, while the cyan, magenta, and blue circles represent the bottom, in-gap, and top edge states. For $r_b = 0.5$ (figure 2(b)), the edge state locates inside the bulk band gap for $r_a < 0.5$, and jumps above the upper band as $r_a > 0.5$; while for $r_b = 1.5$, the edge state remains below the lower band until the band gap closes at $r_a = 1.5$, and appears inside the band gap as r_a further increases. Note that the gap closing line $r_a = r_b$ is not the only condition for phase transition; the edge state also experiences phase changes at $r_b = 1$, when the resonant frequency of the resonator B equals that of the coupling link, which is normalized as 1. Note that this phase transition line would become $r_a = 1$ if the boundary is terminated with resonator A. For example, when r_b sweeps along the line $r_a = 0.5$ (figure 2(d)), the edge state firstly transits from above the upper band to inside the band gap, and then crosses the lower band at $r_b = 1$ to the lower side of the bulk bands. For $r_a = 1.5$ (figure 2(e)), the edge state firstly passes through the upper band from above at $r_b = 1$, and then transits to

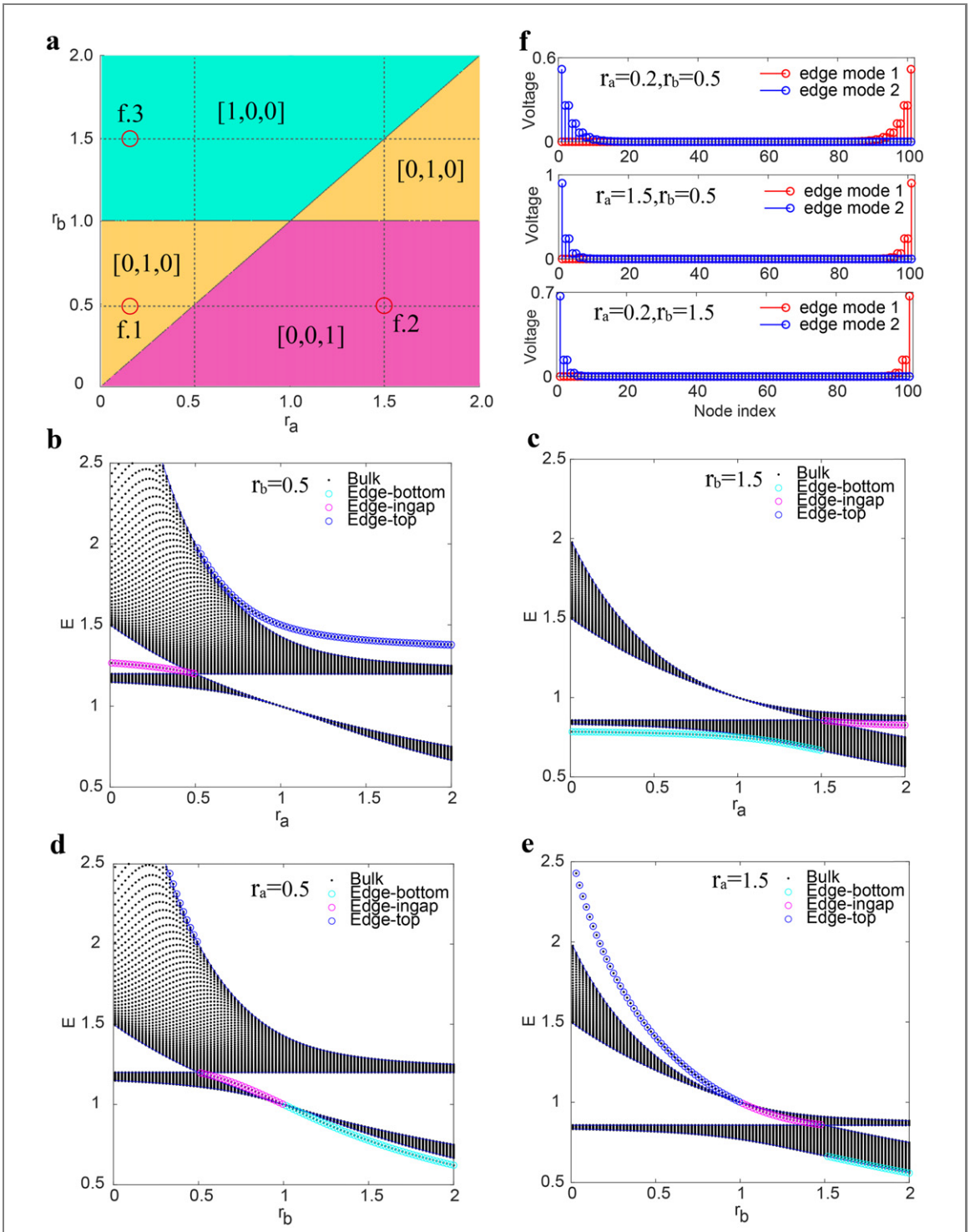

Figure 2. Phase diagram and band structures of the circuit with $s_a = s_b = 1$. (a) Phase diagram as r_a and r_b sweep from 0 to 2. The binary digits '0' and '1' in the bracket represent, from left to right, the existence and absence of spoof topological edge state below, inside, and above the bulk bands, respectively. (b)–(e) Finite band structures obtained along the four gray dashed lines in (a) with (b) $r_b = 0.5$, (c) $r_b = 1.5$, (d) $r_a = 0.5$, (e) $r_a = 1.5$. Black dots and colored circles represent the bulk and edge modes, respectively. (f) Distribution of the edge state on the circuit with parameter sets marked by red circles in (a).

the bottom state at gap closing point $r_b = 1.5$. Figure 2(f) shows the eigenstates of three edge modes [1,0,0], [0,1,0], and [0,0,1] as marked by the circles in figure 2(a), which all exhibit an obvious exponential localization to the edges.

Note that one can find Tamm states transversing across the bulk bands in other systems [36–38]. For example, we can induce a similar surface state in the conventional SSH model by tuning the potential of the boundary sites (see supplementary materials note S4). However, the boundary sites in this case have been intentionally modified to be different from the bulk sites. While in the our circuit, both the boundary sites and bulk sites are kept identical. Most importantly, the phase transition of the edge state observed in the

proposed circuit is strictly dependent on the bulk frequencies, as will be demonstrated in the following section.

3. Analytical solution of the edge state

To further gain a physical insight into the mechanism of the edge state in our electrical circuit, we next consider a more general case with an arbitrary parameter set s_a, s_b, r_a, r_b, and give analytical solutions to its edge mode. To obtain the analytical solution of the edge state, we consider a semi-infinite chain with one end terminated by resonator B. Using the transfer matrix method to obtain the exponential decay ratio of all modes in the bulk circuit and applying it to the boundary, we obtain the equation for solving the edge mode (see supplementary materials note S2),

$$\Xi \cdot \left(E - E_{a,\pi}\right) \cdot \left(E - E_{r,b}\right)^2 = \left(E - E_{b,\pi}\right) \cdot \left(E - E_{0,+}\right)\left(E - E_{0,-}\right) \tag{6}$$

in which $\Xi = (2s_a + t_a) \cdot {t_b}^2 / \{(2s_b + t_b) \cdot (2s_a t_b + 2s_b t_a + t_a t_b)\}$ is a positive real number. Note that $E_{r,b}$ becomes $\left(2s_{b0}^{-1} - s_b^{-1}\right) / (2r_{b0} - r_b)$ in a more general case with arbitrary boundary site L_{b0}, representing a mixed frequency term combining the resonant frequencies of both the bulk and boundary sites. However, for a circuit with natural boundary truncation in our cases, in which the boundary site needs to be kept identical to the bulk site, $E_{r,b}$ is exactly the same as the resonant frequency of resonator B. It is important to note that just because $E_{r,a}$ and $E_{r,b}$ are not relevant to the bulk bands, the transition of the edge state is not solely determined by the bandgap closing condition as in the conventional SSH-type model, as will be demonstrated in the following. They are also of vital importance for the unusual edge state to emerge outside the bulk bands.

It is intriguing to note that equation (6) takes the simple form of the equating between two polynomials with roots equal to five critical frequencies $E_{\pi,a}, E_{\pi,b}, E_{0,+}, E_{0,-}, E_{r,b}$ of the bulk circuit. The status of the edge state, i.e. the existence of edge state and its position relative to the bulk bands, can only change at the crossings of these critical frequencies, that is, when any two elements each from one of the two critical frequency sets $\{E_{\pi,a}, E_{b,r}\}$ and $\{E_{\pi,b}, E_{0,+}, E_{0,-}\}$ are equal to each other. Note that for the case of boundary termination with resonator A, one should replace $E_{b,r}$ on the left side of equation (6) with $E_{a,r}$, and swap $E_{\pi,a}, E_{\pi,b}$. By numerically analyzing the variations of the five critical frequencies in the phase diagram, one can find the following three equations that determine the boundaries of distinct phases in our circuit,

$$E_{b,r} = E_{0,\pm} \Rightarrow t_a = t_b \,(\text{line1}) \tag{7}$$

$$E_{r,b} = E_{0,\pm} = E_{\pi,b} \Rightarrow t_b = 1 \,(\text{line2}) \tag{8}$$

$$E_{\pi,a} = E_{\pi,b} \Rightarrow t_b = \frac{s_b\,(2s_b + 1)}{2s_a + 1} t_a + \frac{s_b\,(2s_a + s_b)}{2s_a + 1} \,(\text{line3})\,. \tag{9}$$

The theoretical prediction of the above critical lines is verified from the phase diagram in figures 3(a) and (b), for two cases with $s_a = 0.5$, $s_b = 1.0$ and $s_a = 1.0$, $s_b = 0.5$, respectively. The phase diagrams in both cases are divided into six regions by the three critical lines. Compared to the phase diagram in figure 2(a) with $s_a = s_b = 1$, the phase diagram in figures 3(a) and (b) exhibit three more new phases [1,1,0], [0,1,1], [0,0,0], which respectively correspond to the following three cases: (1) when the edge state appears both inside and below the bulk bands, (2) it appears both inside and above the bulk bands, and (3) the edge state vanishes. To visualize of the edge mode and its relative position to the bulk band, we sweep the parameter set $[t_a, t_b]$ along a circle (red circle in figures 3(a) and (b)) with radius of 0.5 in the phase diagram. Figure 3(c) shows that as we scan $\theta = \tan^{-1}\left(t_b/t_a\right)$ counterclockwise from $\theta = 0°$, the edge state first appears inside the band gap until θ reaches critical line 1 at 45°. As θ resides between critical line 1 and line 3, the edge state appears both below and inside the bulk band. As θ further increases, the circuit enters phase [1,0,0], with the edge located below the bulk bands. The edge state then crosses from below the lower band into the band gap at $t_b = 1$ (line 2), until it reaches again at line 3, at which the edge state is located both inside and above the bulk bands. As θ passes line 3, the circuit enters into phase [0,0,1], at which the edge state is located above the bulk bands. The phase diagram with parameter set $[s_a, s_b] = [1.0, 0.5]$ (figure 3(d)) is similar to that in the previous case (figure 3(c)), except that critical line 3 is mirrored to the opposite side of critical line 1. This configuration produces a new phase region [0,0,0] between line 1 and line 3, in which the edge state vanishes.

To investigate how the competition of the critical frequencies determines the phase of the circuit, we present in figures 3(e) and (f) the variation of the five critical frequencies as well as the bulk/edge modes as θ scans along the same circular path as in figures 3(c) and (d). It is observed that the crossings of the critical frequency curves correspond exactly to the changes of the edge state in either its existence or position. In

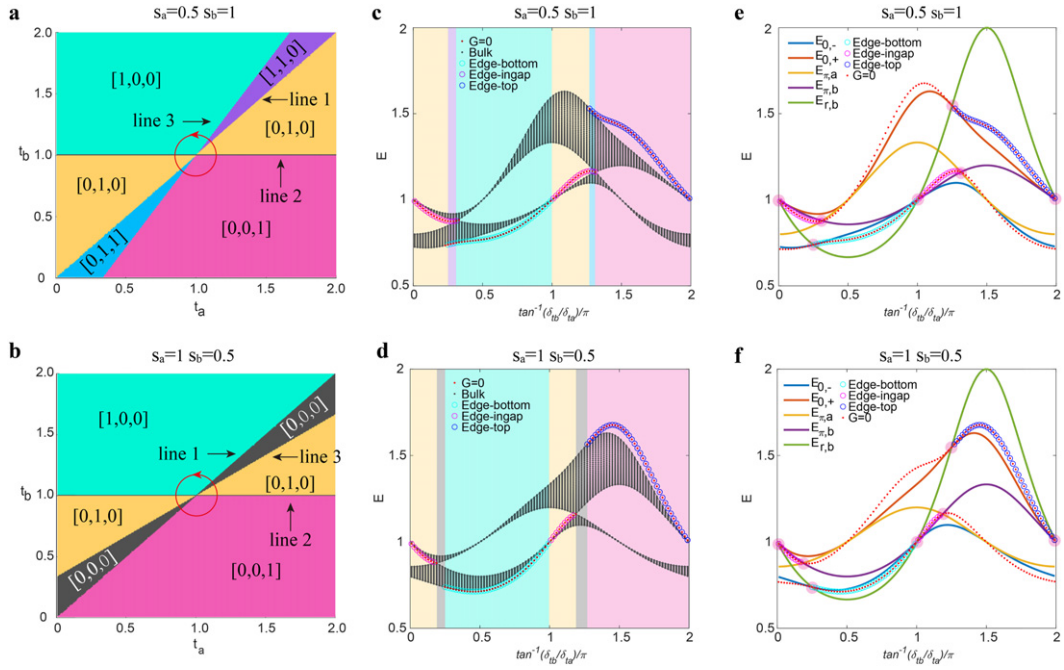

Figure 3. Phase diagram, band structures, and variations of critical frequencies of the circuit with $s_a = 0.5$, $s_b = 1.0$ and $s_a = 1.0$, $s_b = 0.5$. (a) and (b) Phase diagrams of the circuit with $s_a = 0.5$, $s_b = 1.0$ and $s_a = 1.0$, $s_b = 0.5$, respectively. (c) and (d) Band structures of the circuit obtained along the red circles in (a) and (b) with radius of 0.5, respectively. Black dots and colored circles represent the bulk and edge modes, respectively. (e) and (f) Variation of the five critical frequencies along the circle path in (a) and (b), respectively. Red dots indicate all the possible edge modes solved from the edge mode equation equation (6), including both boundary terminations with resonator A and B. All phases are shaded with the same color as in (a) and (b). Those edge states corresponding to boundary termination with site B are selected by using the corresponding decay direction (see supplementary materials note S3) and are marked by colored circles. The red pins mark the crossings of these critical frequencies that correspond to phase transitions.

other words, the existence and position of the edge state remain unchanged as long as the critical frequency curves $E_{\pi,a}(\theta)$, $E_{r,b}(\theta)$ do not cross with $E_{\pi,b}(\theta)$, $E_{0,+}(\theta)$, $E_{0,-}(\theta)$, as marked in figures 3(e) and (f) by small red pins. The continuous red dotted lines represent all the edge mode solutions solved from equation (6). Those red dots marked by circles correspond to the case with boundary terminated by resonator B, while the rest red dots without circles correspond to the case with boundary terminated by resonator A (see supplementary materials note S3). Note that the crossings between the curves $E_{\pi,a}(\theta)$ and $E_{r,b}(\theta)$ do not correspond to phase transitions because both frequencies are on the left-hand side of equation (6).

4. Experimental demonstration

To experimentally verify the existence of the edge state and its transition among the bulk bands, we construct a circuit with 10.5 unit cells (21 nodes), as shown in figure 1(c). C_a/C_b and L_a/L_b are designed as capacitor and inductor sets, which are composed of multiple capacitors/inductors with different capacitance/inductances being connected in parallel to a multiway switching. This configuration allows us to reach all the phases of the circuit as the capacitance C_a/C_b and L_a/L_b can be manually swept from 100 to 2900 pF and 11 to 22 uH, respectively. L_0 and C_0 are fixed at 22 μH and 1000 pF, respectively, during the measurement. This is equivalent to sweep r_a/r_b from 0.1 to 2.9, and s_a/s_b from 0.5 to 1.0. Three different cases, $s_a = 1.0$, $s_b = 1.0$, $s_a = 1.0$, $s_b = 0.5$ and $s_a = 0.5$, $s_b = 1.0$ are chosen for the experiment, which cover all possible types of phase diagrams. In the first case with $L_a = L_b = 22$ μH, figures 4(a) and (b) show the measured and simulated finite band structures as C_a and C_b sweep along a rectangular path as indicated in supplementary figure S1(a). The bulk states are obtained from the impedance spectrum (Z_{11}) measured at node 10 and 11 in the circuit, as indicated by the gray shading in figure 4(a). The red dots represent the edge state which are obtained as the frequency peaks of the impedance spectrum measured at node 1. More experimental details are given in the method. The first point starts from the bottom left corner of the path with C_a/C_b of 300/700 pF, which lies in the [0,1,0] phase with the ingap edge state. As C_a increases, the circuit enters [0,0,1] phase, with the edge state remaining above the upper bulk band. The phase moves back to phase [0,1,0] as C_a reaches 1800 pF and C_b exceeds 1000 pF, as can be observed in figure 4(a) that

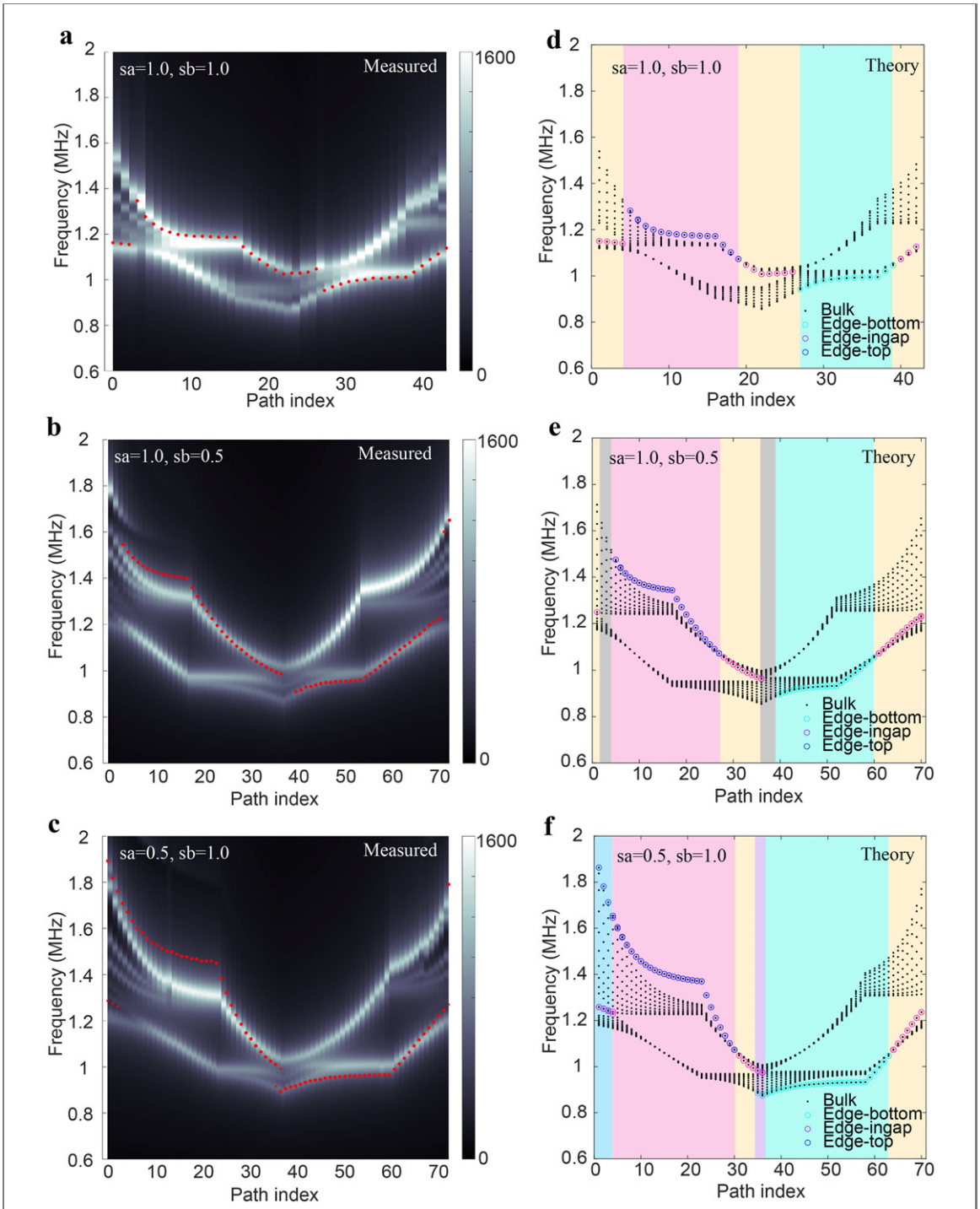

Figure 4. Experimentally measured band structures obtained along a rectangular path in three cases with different configurations of L_a and L_b. (a)–(c) Experimentally measured band structures along the rectangular paths shown in supplementary figures S1(a)–(c) with (a) $s_a = 1.0$, $s_b = 1.0$, (b) $s_a = 1.0$, $s_b = 0.5$. (c) $s_a = 0.5$, $s_b = 1.0$. (d)–(f) Theoretically calculated band structures with the same parameters as in (a)–(c), respectively. All phases in (d)–(f) are shaded with the same color as in supplementary figures S1(a)–(c).

the edge state crosses from above the upper band into the band gap at path index 19. As C_b remains at 1300pF and C_a decreases to 1300 pF (path index 27), the circuit enters phase [1,0,0] with the edge state jumping from inside the bandgap down to the bottom of the lower band. As the parameter sweeps along the left edge of the path back to the starting point, the phase moves back to [0,1,0] with the edge state entering the bandgap at $C_b = 1000$ pF.

For the second case with $s_a = 1.0$, $s_b = 0.5$, two more regions representing the absence of edge state appear in the phase diagram (see supplementary figure S1(b). The sweeping path starts again from the bottom left corner of the rectangular path with C_a/C_b of 200/1000 pF. Those cases with sweeping points falling inside the phase [0,0,0] (gray regions) do not show obvious voltage localization to the circuit edge,

and hence, leading to the absence of red dots in these regions. The frequency spectra of the edge state and bulk state for the other sweeping point follow a similar trend as those in the first case. One may notice that some edge states in case 2 are further away from the bulk states than those in case 1, due to the fact that those points have larger distances to the phase boundaries.

For case 3 with the value of L_a and L_b swapped, the phase diagram displays a new center at $C_a = 2000$ pF and $C_b = 1000$ pF, and two new phase regions [1,1,0] and [0,1,1] (see supplementary figure S1(c). We can see from figure 4(c) that those parameter points inside the [1,1,0] and [0,1,1] regions display two edge states. The position of the edge state relative to the bulk states can be verified from supplementary figure S2, which gives the impedance spectra at all circuit nodes for six parameters chosen in each region in figure 4(c) (marked by yellow circles). The voltage distribution of the edge mode showing the localization of the edge state in each phase region is provided in supplementary figure S3. The measurement results in all three cases (figures 4(a)–(c)) are in excellent agreement with the simulation results (figures 4(d)–(f)).

5. Conclusion

In this work, we present a special kind of edge state in a 1D electrical circuit that mimics the behavior of the topological one. We found that the emergence/vanishing of the edge state and its position relative to the bulk bands in such a Hermitian electrical circuit is uniquely determined by the competition among certain critical frequencies of the bulk circuit, which can be strictly solved from an elegant equation formed by two polynomial functions with roots corresponding exactly to these critical bulk frequencies. Noted that although the trimer model having three sites per unit cell can exhibit similar Tamm state that are controlled by the bulk parameters [39, 40], the circuit proposed in this work composed of only two sites per unit cell serves as the simplest model to exhibit such properties. In addition, the edge states in the proposed circuit can appear outside the bulk bands, while they are confined inside the bandgaps for the trimer model.

We emphasize that the unusual edge state found in our circuit is not the conventional Tamm state, because the emergence and vanishing of Tamm state in quantum electronic and photonic is simply a boundary effect and does not rely on the bulk parameters. Most importantly, there is no literatures reported on the observation of conventional Tamm state to exhibit such topological behaviors. It should also be noted that the unusual edge state shown in this work is neither the SSH-type topological edge state. Because the Chiral symmetry is broken by the unbalanced grounded terms (resonator A and B), Zak phase does not take quantized value (0 and π) for the bulk circuit Hamiltonian in equation (4). However, the fact that the phase of the edge state is ambiguously determined by the order of the bulk critical frequencies can be reasonably viewed, in a broader sense, as the original definition of topology in mathematics, which describes certain quantities that are invariant under continuous deformations. We expect more intriguing physics of the extension of such unusual edge stage to higher-dimensional, and non-Hermitian circuits.

6. Method

6.1. Experimental details

The impedance spectra for each circuit node are measured using a vector network analyser (VNA, Agilent 8753ES) in the S_{11} (reflection coefficient) format with 2 KHz frequency resolution, and is transformed to Z_{11} (input impedance) using $Z_{11} = Z_0 (1 + S_{11}) / (1 - S_{11})$. It can be proved that the impedance Z_{11} measured for a certain circuit node is strictly equivalent to the voltage response on it when excited by an ideal current source on the same node, which does not affect the circuit to be measured and can correctly reflect the permitted mode on the tested node.

Acknowledgments

This work was funded by the European Union's Horizon 2020 Research and Innovation Programme under the Marie Sklodowska-Curie Grant Agreement No. 833797 and Grant No. 777714, the Royal Society, the Wolfson Foundation, Horizon 2020 Action Project No. 734578 (D-SPA), the National Key Research and Development Program of China (Grant Nos. 2017YFA0700201, 2017YFA0700202, 2017YFA0700203), in part by the National Natural Science Foundation of China (Grant Nos. 61631007, 61571117, 61875133, 11874269), and in part by the 111 Project (Grant No. 111-2-05).

Authors' contributions

SL, SJM contributed equally to this work. SL, SJM carried out the analytical modelling, numerical simulations. SL, RWS, and LZ completed the sample fabrication and circuit measurements. As the principal investigators of the projects, SZ, SJM, TJC, and MNC conceived the idea, suggested the designs, planned, coordinated, and supervised the work. BY provides theoretical supports to the work. SL, SJM, and SZ contributed to the writing of the manuscript. All authors discussed the theoretical and numerical aspects and interpreted the results.

Conflict of interest

The authors declare that there are no conflicts of interest regarding the publication of this article.

Data availability statement

The data that support the findings of this study are available upon reasonable request from the authors.

ORCID iDs

Miguel Navarro-Cía https://orcid.org/0000-0003-0256-6465
Tie Jun Cui https://orcid.org/0000-0002-5862-1497

References

[1] Asbóth J K, Oroszlány L and Pályi A 2016 *A Short Course on Topological Insulators* (*Lecture Notes in Physics*) (Berlin: Springer)
[2] Bernevig B A and Hughes T L 2013 *Topological Insulators and Topological Superconductors* (Princeton, NJ: Princeton University Press)
[3] Asbóth J K, Tarasinski B and Delplace P 2014 Chiral symmetry and bulk-boundary correspondence in periodically driven one-dimensional systems *Phys. Rev.* B **90** 125143
[4] Tamm I 1932 On the possible bound states of electrons on a crystal surface *Phys. Z. Sowjetunion* **1** 733–5
[5] Shockley W 1939 On the surface states associated with a periodic potential *Phys. Rev.* **56** 317
[6] Hsu C W, Zhen B, Stone A D, Joannopoulos J D and Soljačić M 2016 Bound states in the continuum *Nat. Rev. Mater.* **1** 16048
[7] Marinica D C, Borisov A G and Shabanov S V 2008 Bound states in the continuum in photonics *Phys. Rev. Lett.* **100** 183902
[8] Dong J, Juricic V and Roy B 2020 Topoelectric circuits: theory and construction (arXiv:2008.11202)
[9] Zhao E 2018 Topological circuits of inductors and capacitors *Ann. Phys., NY* **399** 289–313
[10] Li Z, Wu J, Huang X, Lu J, Li F, Deng W and Liu Z 2020 Bound state in the continuum in topological inductor–capacitor circuit *Appl. Phys. Lett.* **116** 263501
[11] Liu S, Gao W, Zhang Q, Ma S, Zhang L, Liu C, Xiang Y J, Cui T J and Zhang S 2019 Topologically protected edge state in two-dimensional Su–Schrieffer–Heeger circuit *Research* **2019** 8609875
[12] Albert V V, Glazman L I and Jiang L 2015 Topological properties of linear circuit lattices *Phys. Rev. Lett.* **114** 173902
[13] Jia N, Owens C, Sommer A, Schuster D and Simon J 2015 Time- and site-resolved dynamics in a topological circuit *Phys. Rev.* X **5** 021031
[14] Imhof S *et al* 2018 Topolectrical-circuit realization of topological corner modes *Nat. Phys.* **14** 925–9
[15] Lee C H, Imhof S, Berger C, Bayer F, Brehm J, Molenkamp L W, Kiessling T and Thomale R 2018 Topolectrical circuits *Commun. Phys.* **1** 39
[16] Zhu W, Long Y, Chen H and Ren J 2019 Quantum valley Hall effects and spin-valley locking in topological Kane–Mele circuit networks *Phys. Rev.* B **99** 115410
[17] Liu S *et al* 2020 Octupole corner state in a three-dimensional topological circuit *Light: Sci. Appl.* **9** 145
[18] Luo K, Feng J, Zhao Y X and Yu R 2018 Nodal manifolds bounded by exceptional points on non-Hermitian honeycomb lattices and electrical-circuit realizations (arXiv:1810.09231)
[19] Zhang W, Zou D, He W, Bao J, Pei Q, Sun H and Zhang X 2020 Topolectrical-circuit realization of 4D hexadecapole insulator (arXiv:2001.07931v1)
[20] Yu R, Zhao Y X and Schnyder A P 2019 A genuine realization of the spinless 4D topological insulator by electric circuits (arXiv:1906.00883)
[21] Li L, Lee C H and Gong J 2019 Boundary states of 4D topological matter emergence and full 3D-imaging of nodal Seifert surfaces (arXiv:1905.07069)
[22] Ezawa M 2019 Electric circuit simulations of nth-Chern insulators in $2n$-dimensional space and their non-Hermitian generalizations for arbitral n (arXiv:1905.10734)
[23] Stegmaier A *et al* 2020 Topological defect engineering and PT-symmetry in non-Hermitian electrical circuits (arXiv:2011.14836v1)
[24] Lu Y, Jia N, Su L, Owens C, Juzeliūnas G, Schuster D I and Simon J 2019 Probing the Berry curvature and Fermi arcs of a Weyl circuit *Phys. Rev.* B **99** 020302
[25] Li R, Lv B, Tao H, Shi J, Chong Y, Zhang B and Chen H 2019 Ideal type-II Weyl points in topological circuits (arXiv:1910.03503v1)
[26] Rafi-UI-Islam S M, Siu B Z and Jalil M B A 2019 Transport across a topoelectrical Weyl semimetal heterojunction (arXiv:1908.03642v1)

[27] Ezawa M 2018 Higher-order topological electric circuits and topological corner resonance on the breathing kagome and pyrochlore lattices *Phys. Rev.* B **98** 201402
[28] Ezawa M 2019 Non-Hermitian boundary and interface states in nonreciprocal higher-order topological metals and electrical circuits *Phys. Rev.* B **99** 121411
[29] Hadad Y, Soric J C, Khanikaev A B and Alu A 2018 Self-induced topological protection in nonlinear circuit arrays *Nat. Electron.* **1** 178–82
[30] Hadad Y, Vitelli V and Alu A 2017 Solitons and propagating domain walls in topological resonator arrays *ACS Photonics* **4** 1974–9
[31] Wang Y, Lang L-J, Lee C H, Zhang B and Chong Y D 2019 Topologically enhanced harmonic generation in a nonlinear transmission line metamaterial *Nat. Commun.* **10** 1102
[32] Wu Z *et al* 2016 Realization of two-dimensional spin–orbit coupling for Bose–Einstein condensates *Science* **354** 6308
[33] Osterloh K, Baig M, Santos L, Zoller P and Lewenstein M 2005 Cold atoms in non-abelian gauge potentials: from the Hofstadter 'moth' to lattice gauge theory *Phys. Rev. Lett.* **95** 010403
[34] Jacob A, Öhberg P, Juzeliūnas G and Santos L 2007 Cold atom dynamics in non-abelian gauge fields *Appl. Phys.* B **89** 439
[35] Song Z, Wu T, Wu W and Yu R 2020 Experimental realization of non-abelian gauge potentials and topological Chern state in circuit system (arXiv:2009.04870)
[36] Malkova M, Hromada I, Wang X, Bryant G and Chen Z 2009 Transition between Tamm-like and Shockley-like surface states in optically induced photonic superlattices *Phys. Rev.* A **80** 043806
[37] Blanco-Redondo A, Andonegui I, Collins M J, Harari G, Lumer Y, Rechtsman M C, Eggleton B J and Segev M 2016 Topological optical waveguiding in silicon and the transition between topological and trivial defect states *Phys. Rev. Lett.* **116** 163901
[38] St-Jean P, Goblot V, Galopin E, Lemaître A, Ozawa T, Le Gratiet L, Sagnes I, Bloch J and Amo A 2017 Lasing in topological edge states of a one-dimensional lattice *Nat. Photon.* **11** 651
[39] Alvarez V M M and Coutinho-Filho M D 2019 Edge states in trimer lattices *Phys. Rev.* A **99** 013833
[40] Huda M N, Kezilebieke S, Ojanen T, Drost R and Liljeroth P 2020 Tuneable topological domain wall states in engineered atomic chains *npj Quantum Mater.* **5** 17